Nanoscale

COMMUNICATION

View Article Online
View Journal | View Issue

Cite this: *Nanoscale*, 2017, **9**, 18194

Received 16th September 2017,
Accepted 21st October 2017

DOI: 10.1039/c7nr06902b

rsc.li/nanoscale

Self-assembled nano-leaf/vein bionic structure of TiO_2/MoS_2 composites for photoelectric sensors†

Qianyu Wang,[a] Peng Yu,[a] Lu Bai,[a] Ruiying Bao,[a] Ning Wang,[b] Chuanbing Cheng,[c] Zhengying Liu,[a] Mingbo Yang,[a] Wei Yang *[a] and Zhanhu Guo *[c]

Inspired by the leaf/vein structure of leaves which effectively supports the photosynthesis of green plants, a nano-leaf/vein bionic structure of self-assembled TiO_2/MoS_2 composites is applied to induce the reversible photochromic reactions of methylene blue (MB) for the first time. This reversible photochromic phenomenon gives a novel performance for the TiO_2/MoS_2 composites and expands their applications. Similar to the case where the natural vein network in leaves ensures the efficient material transfer and energy exchange for photosynthesis, the bionic internal MoS_2 vein network in the composites ensures the efficient separation and directional transfer of photo-generated carriers to restrain the photocatalytic degradation reactions and to enhance the reversible photochromic reactions. Furthermore, the photosensitive applications of the TiO_2/MoS_2/MB systems with such a self-assembled nano-leaf/vein bionic structure are discussed with two typical photoelectric sensory models for both controllers and detectors.

1. Introduction

Among the core sensory systems, photoelectric sensors show clear advantages such as high accuracy, rapid response and favorable stability, owing to their easy control by an artificial light source, fast detection of light change without physical contacts, and quick responses.[1] A typical photoelectric sensor is made up of three major elements, *i.e.*, a luminous element, a photosensitive element and a transition element. Photosensitive elements convert photosignals or photoinduced variates from luminous elements to physical quantity signals, and finally to electrical signals through transition elements. Thus, the photosensitive element is the most important part that acts as a bridge to connect the luminous element and the transition element to ensure the transformation and transmission of signals. Nowadays, the most widely applied photosensitive elements are photosensitive resistors from various semiconductive materials, which give different resistances under lumination.[2]

Methylene blue (MB) is a typical redox dye and exhibits a series of interesting color switching (bright blue to colorless) reactions through gaining or losing electrons. With this unique property, MB can be combined with semiconductors to form a reversible photochromic system.[3] In this system, the role of the semiconductor is to absorb light and offer photo-generated electrons (e^-). Semiconductive TiO_2, with its excellent photoelectrochemical activity,[4,5] has been studied in photocatalysis[6–8] and electrochemistry[9–11] including reversible photochromic systems with MB.[12–15] The irreversible photocatalytic degradation reaction and reversible color switching reaction are competing reactions. To ensure color switching, the photocatalytic degradation reactions must be restrained.[13] In previous reports, this was generally realized by restraining the generation of a hydroxyl radical (*OH) produced by photo-generated holes (h^+) and the reaction between the hydroxyl radical and the MB solution.[16]

A typical MB photochromic system, usually containing a MB solution, a semiconductor material (such as TiO_2), and a sacrificial electron donor (SED, such as poly(ethylene glycol)-*b*-poly(propylene glycol)-*b*-poly(ethylene glycol)), has been used as an oxygen indicator.[17,18] In this case, when TiO_2 produces photo-generated electrons and holes under UV light irradiation, the freely diffusing holes react with the SED. Meanwhile, both low pH[13,15] and low oxygen content[14,19] can promote the decoloration process of MB in the TiO_2/MB system. O_2 has been proved not to be a prerequisite but in that case the role of the SED and strong acidic conditions is indispensable, and the SED material must composite with TiO_2 well.[16] Many efforts have been made to release the system from the external SED but some other materials with SED-like functions such as

[a]College of Polymer Science and Engineering, State Key Laboratory of Polymer Materials Engineering, Sichuan University, Chengdu 610065, Sichuan, China. E-mail: weiyang@scu.edu.cn
[b]Engineered Multifunctional Composites (EMC) Nanotechnology LLC, Knoxville, TN 37934, USA
[c]Integrated Composites Laboratory (ICL), Department of Chemical & Biomolecular Engineering, University of Tennessee, Knoxville, TN 37996, USA. E-mail: zguo10@utk.edu

†Electronic supplementary information (ESI) available. See DOI: 10.1039/c7nr06902b

colloidal barium-dopant TiO_2 nanocrystals which can produce oxygen vacancies are still needed to consume the photo-generated holes.[20,21] In other words, all the previous studies allowed the photo-generated holes to diffuse to the surface of the materials freely and then tried to consume them by using some kinds of SED or SED-like materials.

MoS_2 with a narrower band gap (1.9 eV) compared with that of TiO_2 (3.2 eV)[22,23] has been loaded into TiO_2 to enhance its photocatalytic activity[24,25] because it can form a new heterostructure with TiO_2.[26–28] This heterostructure can realize a directional transfer of photo-generated carriers under illumination, *i.e.*, the transfer of all photo-generated holes to the valence band of MoS_2 and the simultaneous transfer of all photo-generated electrons to the conduction band of TiO_2.[29,30] Although TiO_2/MoS_2 composites (TM) have been reported as photocatalysts for water pollutant degradation[26,31–34] and water splitting hydrogen production,[24,35–38] their applications in inducing the reversible photochromic reactions of MB have never been reported. Without MoS_2, the TiO_2/MB systems are mostly applied in ink-free light-printing.[21,39,40]

Inspired by nature that created the leaf/vein structure of green plant leaves which effectively supports photosynthesis, a novel nano-leaf/vein bionic heterostructure of TM (Fig. 1) was designed and prepared *via* a facile self-assembly method to realize rapid color switching and to restrain the photocatalytic degradation reactions of MB for the first time, which is a novel performance for the TiO_2/MoS_2 composites. Based on such a performance, the resulting TiO_2/MoS_2-MB system has a high probability of being used as a photosensitive element in photoelectric sensors and the application of TiO_2/MoS_2 composites can be expanded.

In the preparation of TiO_2/MoS_2 composites with the nano-leaf/vein bionic structure, the TiO_2 nanoparticles were used to simulate the mesophyll cells and the MoS_2 nano-silks to simulate the veins. In natural leaves, the veins stretch, bifurcate and cross between mesophyll cells and build an extremely efficient network to realize material transportation and energy conversion for the biochemical reactions of photosynthesis. Similarly, in this work, the internal network made up of MoS_2 veins can not only endow the composites with a high quantum efficiency through the efficient separation of photo-generated carriers, but also directionally transfer the photo-generated holes to the center of composites to significantly slow down and restrain the generation of hydroxyl radicals and further restrain the photocatalytic degradation reaction of MB. Both effects can enhance the color switching reactions of MB effectively.

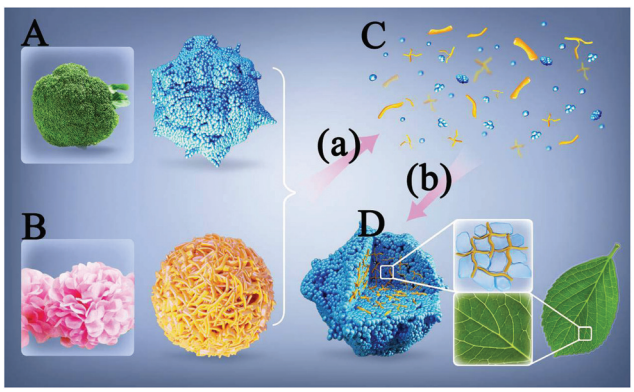

Fig. 1 A schematic illustration of the TiO_2/MoS_2 composites with a nano-leaf/vein bionic structure prepared by using the self-assembly method. (A) TiO_2 nano-broccoli; (B) MoS_2 nano-hyacinth; (C) homogeneous suspension of TiO_2 particles and MoS_2 silks; (D) nano-leaf/vein bionic structure of TiO_2/MoS_2 composites; (a) a mechanical high-speed dispersion process; (b) the self-assembly of the homogeneous suspension of TiO_2 particles and MoS_2 silks after high-speed shearing.

2. Experimental section

2.1 Synthesis of MoS_2 nano-hyacinth

One mmol sodium molybdate ($Na_2MoO_4{\cdot}2H_2O$, S104867, Aladdin, Shanghai, China) and 5 mmol thiourea (T112514, Aladdin, Shanghai, China) were dissolved in 60 mL distilled water. The homogeneous solution was stirred for 30 min and then transferred into a 100 mL Teflon-lined autoclave at 210 °C for 12 h. After washing with deionized water, centrifugation, and drying at 60 °C for 24 h, the black powder of MoS_2 nano-hyacinth was collected.

2.2 Synthesis of the nano-leaf/vein bionic structure of TiO_2/MoS_2 composites

Anatase phase TiO_2 nano-broccoli (T104943, Aladdin, Shanghai, China) and the obtained MoS_2 nano-hyacinth, with a combined mass of 200 mg (Table S1†), were dispersed in 20 mL absolute ethyl alcohol, and then the mixed solution was dispersed using a high-speed dispersing mixer (XHF-DY, XinZhi Biotech, Ningbo, China) at a speed of 10 000 rpm for 10 min. After this, the mixed solution of composites was directly used in the color switching experiment.

2.3 Color switching experiment

The color switching experiment was conducted using a xenon lamp photocatalytic reaction system (CEL-HXUV300, Au-light, Beijing, China). Typically, 20 mL mixed solution of composites was added into 200 mL MB solution (20 mg L^{-1}), and the TM/MB system was irradiated with simulated solar light to allow it to be bleached and then the light was turned off to recover to blue. The solution was kept under constant stirring and at 20 °C by using a thermostatic water-jacket during the experiment. 3 mL sample was taken at equal time intervals, and then the absorption intensity at 664 nm was recorded using a UV-vis spectrophotometer (UV-3600, Shimadzu, Japan) after removing the composites. Each sample was tested through a cycle of decoloration and recoloration processes. Because of the linear relationship between the concentration and the absorbance at the absorption peak (664 nm) of the visible light wave band of the MB solution (Fig. S6†), the absorbance can be detected by using a UV-vis spectrophotometer and is used to determine the concentration of MB (C) in the system.

3. Results and discussion

The TiO_2 nano-broccoli (Fig. 1A & Fig. S1a†) and MoS_2 nano-hyacinth (Fig. 1B & Fig. S1b†) were selected as the raw materials to offer TiO_2 nanoparticles and MoS_2 nano-silks, and a high-speed dispersing mixer (Fig. 1(a)) was used to achieve a homogeneous suspension of the nanoparticles and nano-silks (Fig. 1C). The good suspension state was very unstable. Once the mixing operation was stopped, the suspended nanoparticles and nano-silks quickly rejoined into particle clusters, driven by the high surface energy of good dispersion and suspension. In this process, the nano-leaf/vein bionic structure of TM (Fig. 1D) was built with MoS_2 nano-silks inserted between the TiO_2 nanoparticles (Fig. 1(b)), and the vein structure can be regulated by loading different contents of MoS_2 nano-silks.

Fig. 2 shows the morphology of the raw materials (Fig. 2A and B) and the nano-leaf/vein bionic structure of TM (Fig. 2C–H) with different MoS_2 contents (TM05–30 means that the MoS_2 content is from 5 to 30 wt%). The MoS_2 veins were marked in bright yellow lines. The TiO_2 nanoparticles were observed to form dense clusters like the mesophyll cells (Fig. 2A) and the MoS_2 nano-silks stretched like leaf veins (Fig. 2B). In TM05 (Fig. 2C), a few MoS_2 veins were observed and the veins were stretched and bifurcated, but not crossed; while in TM10 (Fig. 2D), more MoS_2 veins were observed and the veins began to cross with each other and formed a loose network. When the content of MoS_2 increased to 20 wt% (sample TM20, Fig. 2E and F), it was surprising to note that many MoS_2 veins stretched, bifurcated between TiO_2 nanoparticles and crossed with each other to form a good nano-network. However, with a further increase in the MoS_2 content to 30 wt%, instead of forming an even denser nano-leaf/vein structure, the MoS_2 veins in the center areas of the TM30 composites tended to gather into bundles of thicker veins (Fig. 2G), and some MoS_2 veins at the border areas of the TM30 composites (Fig. 2H) reached out of the surface. Excess MoS_2 nano-silks are observed to begin to cover the surface of the composites (areas in the bright green circles, Fig. S2†). Thus, at a higher content of MoS_2 up to 30 wt%, the MoS_2 in the composites cannot be described as internal vein networks anymore.

Fig. 3 shows the color switching performance of the composites. The TM05/MB system was bleached out in 4 min, and then recolored in 10 min, with 12% degradation (Fig. 3A, pink illustration), indicating that the internal MoS_2 veins restrained the photocatalytic degradation reaction of MB to some extent. It is worth noting that under the same conditions, the pure TiO_2 sample needs 30 min to photocatalytically degrade MB thoroughly (Fig. S3d†); thus it can be concluded that the color switching reactions are much faster than the photocatalytic degradation reactions.[38] The TM10/MB system was bleached out in 2 min, and then recolored in 4 min, with only 4% degradation (Fig. 3A, orange illustration); the TM20/MB system was bleached out as fast as 0.5 min, and then recolored in just 1 min, with merely 2% degradation (Fig. 3A, green illustration). These results demonstrate that with the formation and perfection of the internal MoS_2 vein network in the composites, both the decoloration and recoloration processes of the color switching reactions were greatly promoted, and the photocatalytic degradation reaction was significantly slowed down and even restrained at the same time (Fig. 3B).

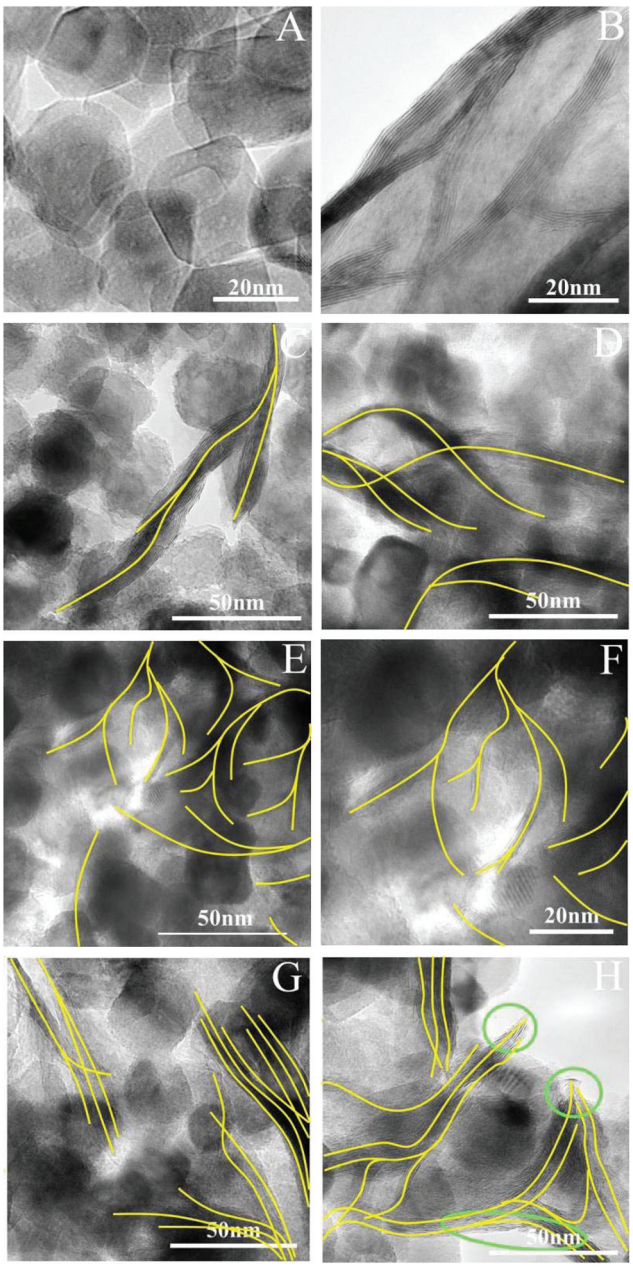

Fig. 2 TEM images of (A) TiO_2 nano-broccoli; (B) MoS_2 nano-hyacinth; (C) TM05; (D) TM10; (E), (F) TM20 with different magnifications and the inner MoS_2 vein structure (G) and the MoS_2 veins reaching out of the surface (H) of TM30 composites. All the MoS_2 veins are marked in yellow lines to facilitate observation.

Taking the test error into account, cyclic tests were performed to see whether the photocatalytic degradation reactions were restrained successfully (Fig. 3C, Fig. S4 and S5†). After 10 cycles (Fig. 3C) and even 20 cycles (Fig. S4†), the con-

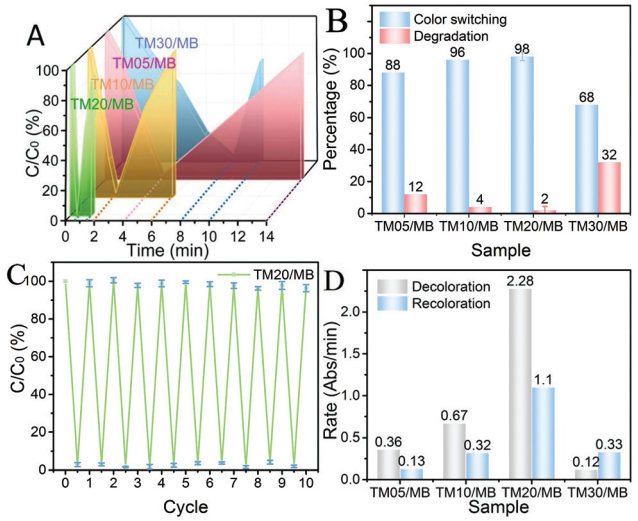

Fig. 3 Color switching: (A) the decoloration and recoloration processes of the samples with respect to time; the original data are shown in Fig. S9;† (B) color switching/degradation percentage of the samples; (C) cyclic test of TM20/MB; (D) color switching rate of the samples. C/C_0: the ratio of the tested concentration and the original concentration of MB; rate: the absorbance change in a decoloration or recoloration process (Abs) within the consumed time (min).

centration of MB in TM20/MB was still maintained very close to the initial value, while after only 10 cycles, the concentration of MB in TM10/MB showed a clear drop (Fig. S5†) with about 9.7% of MB degraded. This result clearly demonstrates that only the TM20 composites can effectively restrain the photocatalytic degradation reaction of MB.

However, the TM30/MB system took 8 min to bleach out but only 2 min to recover (Fig. 3A, blue illustration) and the degradation percentage of MB was up to 32%. Apparently, the TM30 composites cannot restrain the photocatalytic degradation reaction of MB because the MoS_2 veins stretch out of the surface of composites and ruin the directional transferring effect of the internal MoS_2 vein network on the photo-generated carriers. These stretched-out MoS_2 veins can even promote the photocatalytic degradation, and in this case, the composite structure is just like the core–shell TiO_2–MoS_2 structures that were designed for better photocatalytic activity and applied for enhancing the photocatalytic degradation reactions.[26,32] The recoloration process of the TM30/MB system seems to be much faster due to the 66% degradation-induced decrease of the entire MB content (Fig. 3B) after the first bleaching process.

The rates of the decoloration/recoloration process of the samples were also calculated based on the absorbance change in a decoloration or recoloration process and the consumed time (Fig. 3D). The results demonstrated that the formation of the internal MoS_2 vein network could sharply increase the rate of both the decoloration and recoloration processes, which also clearly proved the extremely high quantum efficiency of the designed nano-leaf/vein bionic structures. Compared with the TiO_2/MB systems reported previously,[16,39] such a nano-leaf/vein bionic structured TM/MB system shows a rapid color recovery rate as high as 1.1 Abs min^{-1}, much higher than other samples (Fig. 3D) without any light illumination or extra heating. Because the photocatalytic degradation was not well restrained in the TM30/MB system, the color switching rate was very low. Besides this, bulk MoS_2 (Fig. S3a and b†) was also used to replace MoS_2 nano-hyacinth and to prepare a control sample for the TM20 composites, but only a not well-composited structure (Fig. S3c†) with a slightly enhanced photocatalytic degradation was obtained (Fig. S3d†).

With such an excellent color switching performance, the TM20/MB system can be used as a photosensitive element in photoelectric sensors (Fig. 4A). Devices of different sizes can be built (Fig. 4A(a)) according to the requirements of practical applications. In particular, this TM20/MB system shows clear advantages in microminiaturization, which gives the TM20/MB system great potential to be used in micron and precise sensors. Furthermore, the color switching performance is impregnable after scaling (Fig. 4A(b)). A typical photoelectric sensor can be constructed by combining the TM20/MB system with a photosource and a photometer (Fig. 4B(a)), and the sensor can realize the transformation of signals (Fig. 4B(b)). This modularized method will certainly endow the system with more flexibility in applications.

Practically, there are mainly two types of photoelectric sensors, *i.e.*, controllers and detectors. For controllers, the photosensitive element transforms controllable photosignals to the given electric signals to control the targets, while for detectors, the photosensitive element detects the photosignals transformed from the electric signals given by the target. For each type, a typical sensory model was given to expound the practical applications of the TM20/MB system. "*A*" means the absorbance value of the TM20/MB system, and "ΔA" means the rate of change of "*A*". "*A*" can be measured by using a photometer every second, and "ΔA" per second can be calculated at the same time.

In the controller model (Fig. 4C(a)), the TM20/MB system can be used to control the traffic light circuit (Fig. 4C(b)). In each cycle of the system, when "*A*" changes from 1.6 (the absorbance value of 20 mg L^{-1} MB according to Fig. S6†) to 0, and then recovers from 0 to 1.6, the red, yellow and green traffic lights can be turned on and off successively. This process can also be suspended to maintain a signal without any energy consumption, unlike the case where the photodiode needs a sustaining extra illumination and electricity to hold a signal.

In the detector model (Fig. 4D), because of the linear relationship between the rate of change of absorbance "ΔA" and the optical power density "*B*" (Fig. S7†), if there exists any other physical quantity "*C*" which can lead to a change of "*B*" and has a relation with "*B*", then a relationship between "*A*" and "*C*" can be constructed, where "*C*" is the goal to be detected. Then, all we need to do is just to detect the rate of change of absorbance of the TM20/MB system, and the value of "*C*" can be easily detected immediately. Considering so many "*C*" in this world, such as the material concentration,

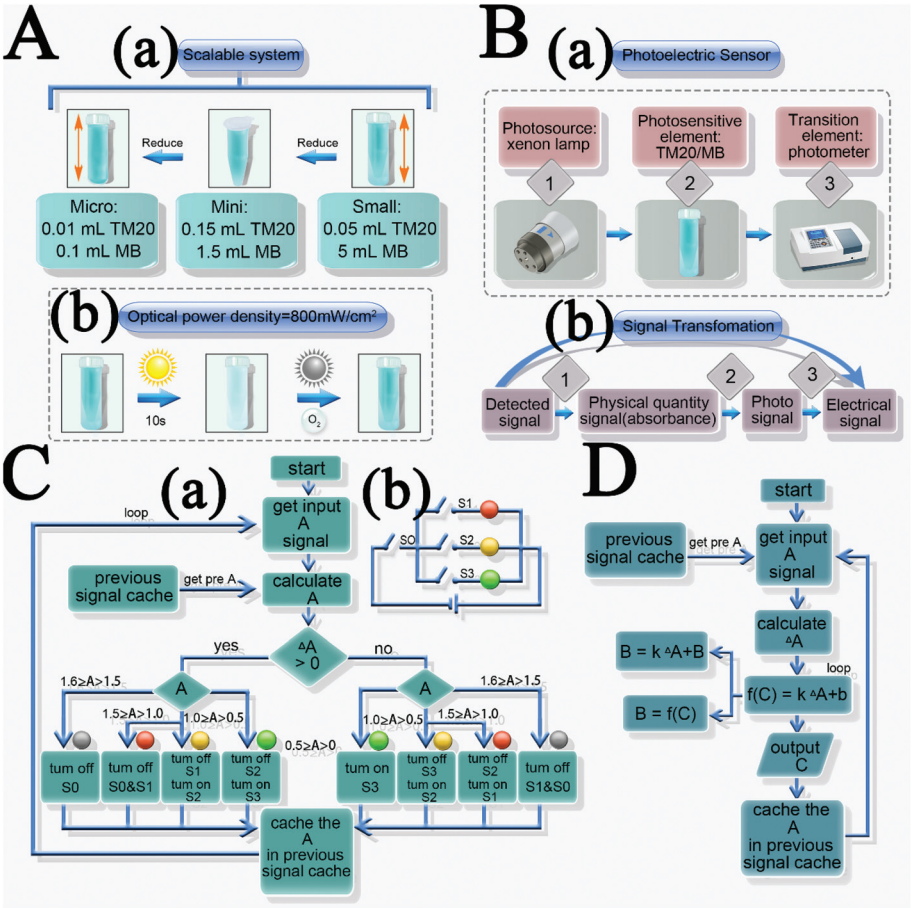

Fig. 4 (A) The size scalability of TM20/MB systems. (a) Systems in different sizes can exhibit an excellent color switching performance; (b) the color switching of a microsystem which can be easily introduced into microcontrollers or microdetectors. (B) A typical example of a photoelectric sensor. (a) The assembly of the sensor and (b) the signal transformation in the sensor. (C) (a) An application model of a typical controller and (b) a traffic light circuit controlled by the controller; (D) an application model of a typical detector.

the density in the light path, the size of objects which can reflect light, the distance between a light absorption object and a light source, *etc.*, all the parameters of "*C*" can be detected with the model described in Fig. 4D.

Fig. 5 illustrates the working mechanism of TM with such a nano-leaf/vein bionic structure. MB exhibits a series of interesting color switching arising from its reversible redox reactions (Fig. 5A). The oxidized form of MB (Fig. 5A(a)) is bright blue, while the reduced form of MB (Fig. 5A(b), also called leuco-methylene blue, LMB) is colorless. MB can be reduced to LMB through a simple and rapid one-step reaction which can easily take place when combining with electrons (e^-) (Fig. 5A (c)), and this reaction leads to the decoloration of MB. However, LMB is unstable and can turn back to MB upon releasing electrons to oxidizing agents such as O_2 (Fig. 5A(d)), and this recoloration process happens effortlessly when LMB is exposed to air. So, all the color switching reactions are reversible and circulatory without any MB consumption.

MoS_2 can form a new heterostructure with TiO_2 (Fig. 5B & S8†).[26–28] Before composition, both the conduction band (CB) edge and the Fermi level of TiO_2 (*vs.* standard hydrogen electrode) are higher than that of MoS_2 (TiO_2: −0.3 V; MoS_2: −0.1 V) (Fig. S8A†). After composition, the Fermi level of TiO_2 moves down (Fig. S8B(a)†) while that of MoS_2 moves up (Fig. S8B(b)†) until a new balance is realized (TiO_2: −0.2 V; MoS_2: −0.3 V). Meanwhile, the entire energy band of TiO_2 decreases and that of MoS_2 increases with the change in the Fermi level. Finally, the CB edge of TiO_2 is lower than that of MoS_2. After reaching the balance, an internal electric field is formed, in which TiO_2 is positively charged (Fig. S8B(c)†) while MoS_2 is negatively charged (Fig. S8B(d)†). Under light irradiation, both components excite photo-generated electrons and holes. With the promotion of the internal electric field (Fig. 5B(a and b)), the excited holes on the valence band (VB) of TiO_2 transfer to that of MoS_2 while the excited electrons remain in the CB of TiO_2 (Fig. 5B(c)). Corresponding to this process, the excited electrons on the CB of MoS_2 transfer to that of TiO_2 while the excited holes remain in the VB of MoS_2 (Fig. 5B(d)).[29,30] As a result, all the holes are transferred to MoS_2 simultaneously and all the electrons are transferred to TiO_2. Through this process, the internal MoS_2 vein network structure can realize the directional transfer of photo-gener-

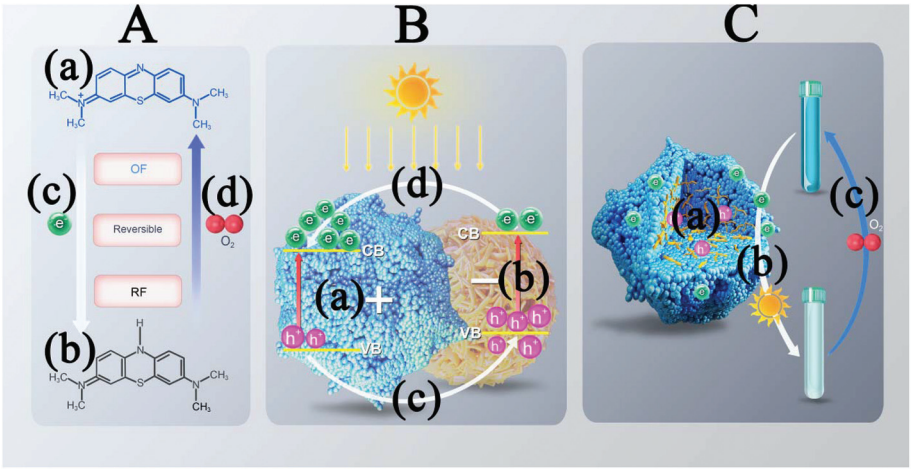

Fig. 5 (A) Reversible photochromic reactions of methylene blue (MB, a) in the oxidized form (OF) and the reduced form (RF) of MB (LMB, b) through reduction (c) and oxidation (d); (B) the heterostructure of TiO_2/MoS_2 composites, (a) (b) the internal electric field, (c) the transfer of photo-generated holes and (d) the transfer of photo-generated electrons; (C) the reaction mechanism of the nano-leaf/vein bionic structure of TiO_2/MoS_2 composites: (a) the directional transfer of photo-generated carriers of the inner vein-like network of MoS_2, (b) the photo-generated electrons inducing the decoloration of MB and (c) the recoloration of LMB induced by O_2.

ated carriers (Fig. 5C(a)) and it is worth noting that only the internal MoS_2 network structure can realize that, which means that the loaded MoS_2 must form a network and no MoS_2 is exposed on the surface of the composites.

The irreversible photocatalytic degradation reaction and reversible color switching reaction are the two main competing reactions in the TM/MB system, both happening at the surface of the TiO_2/MoS_2 composites. For the photocatalytic degradation reaction, if one photo-generated hole reaches the surface, it will react with one OH^- from the water firstly to generate one hydroxyl radical, and then the generated hydroxyl radical will degrade MB by breaking its chemical bonds step by step through a series of oxidizing reactions. This process needs quite a few photo-generated holes to generate a sufficient amount of hydroxyl radicals to degrade one MB molecule into CO_2 and H_2O. So the photocatalytic degradation reaction is a multistep, slow and difficult reaction, and the degradation of one MB molecule will consume many photo-generated holes. However, for the color switching reaction, if one photo-generated electron reaches the surface, it can directly combine with one MB molecule, and then convert it to one colorless LMB molecule easily. So the color switching reaction is a one-step, fast and easy reaction,[41] and the decoloration of one MB molecule only consumes one photo-generated electron.

Once the TM/MB system is under light irradiation, both TiO_2 and MoS_2 excite photo-generated electrons and holes. Because the internal MoS_2 vein network structure can directionally transfer photo-generated carriers, the photo-generated electrons will transfer freely and easily to the surface of the outer TiO_2 nanoparticles and get fully exposed to the MB solution, and then efficiently reduce the absorbed MB to LMB (Fig. 5C(b)). But it is difficult for the photo-generated holes to reach the surface because the internal electric field will push them to the center of the composites. Certainly, some photo-generated holes can still reach the surface, generate hydroxyl radicals and degrade MB, but before they can degrade a certain amount of MB, the vast majority of MB molecules in the solution have already combined with enough photo-generated electrons and become colorless LMB molecules. When the light is turned off, both the photocatalytic degradation reaction and the color switching reaction cannot continue anymore, and the LMB molecules will turn back to the MB molecules through the oxidation of O_2 in the solution (Fig. 5C(c)). For each color switching cycle, only a negligible number of MB molecules are degraded by the hydroxyl radicals in time before the entire solution is bleached by the photo-generated electrons. In this way, the degradation reaction is "restrained" macroscopically, and the color switching reaction can circulate stably many times without any visible consumption of MB. In addition, because MoS_2 also prevents the recombination of electrons and holes,[42] the decoloration process of MB can be further enhanced.

4. Conclusion

A novel TiO_2/MoS_2 nano-leaf/vein bionic structure was prepared through a facile and efficient self-assembly method to enhance the reversible photochromic reactions of MB for the first time. The obtained structure shows an extraordinarily high quantum efficiency and can vastly enhance the decoloration and recoloration processes of MB, and it also restrains the photocatalytic degradation almost thoroughly by directionally transferring the photo-generated carriers through the internal MoS_2 veins. This bionic structure is so effective that all the color switching reactions can be operated in a neutral solution and in air without loading any kind of SED. Inducing the

reversible photochromic reactions of MB by the TiO_2/MoS_2 composites for the first time gives a novel performance and possible application to these composites. Based on such a performance, the TM20/MB system can be used as a photosensitive element in photoelectric sensors, and with its excellent performance and flexible application model, this novel system holds great potential in practical applications such as controllers and detectors.

Conflicts of interest

The authors declared that they have no conflicts of interest to this work.

Acknowledgements

This research was financially supported by the National Natural Science Foundation of China (NNSFC Grant No. 51422305 and 51421061), the Sichuan Provincial Science Fund for Distinguished Young Scholars (2015JQO003), and the State Key Laboratory of Polymer Materials Engineering (Grant No. sklpme2014-2-02).

References

1 C. J. Zheng, *Intelligence Computation and Evolutionary Computation*, Springer, Berlin, Heidelberg, 2013, vol. 180, pp. 671–677.
2 J. H. Li, L. Y. Niu, Z. J. Zheng and F. Yan, *Adv. Mater.*, 2014, **26**, 5239–5273.
3 H. Yoneyama, H. Tamura and Y. Toyoguch, *J. Phys. Chem.*, 1972, **76**(23), 3460.
4 X. Xu, Z. Y. Fan, S. J. Ding, D. M. Yu and Y. P. Du, *Nanoscale*, 2014, **6**(10), 5245–5250.
5 Z. Q. Liu, X. H. Cao, B. Wang, M. Xia, S. Lin, Z. H. Guo, X. M. Zhang and S. Y. Gao, *J. Power Sources*, 2017, **342**, 452–459.
6 K. S. Ranjith and T. Uyar, *J. Mater. Chem. A*, 2017, **5**(27), 14206–14219.
7 L. Zhang, W. Yu, C. Han, J. Guo, Q. H. Zhang, H. Y. Xie, Q. Shao, Z. G. Sun and Z. H. Guo, *J. Electrochem. Soc.*, 2017, **164**(9), H651–H656.
8 Y. M. Zhao, Y. Z. Dong, F. T. Lu, C. G. Ju, L. Liu, J. Zhang, B. Zhang and Y. Q. Feng, *J. Mater. Chem. A*, 2017, **5**(29), 15380–15389.
9 S. M. Guo, J. R. Liu, S. Qiu, W. Liu, Y. R. Wang, N. N. Wu, J. Guo and Z. H. Guo, *J. Mater. Chem. A*, 2015, **3**(47), 23895–23904.
10 B. Chen, N. Q. Zhao, L. C. Guo, F. He, C. S. Shi, C. N. He, J. J. Li and E. Z. Liu, *Nanoscale*, 2015, **7**(30), 12895–12905.
11 X. M. Lou, C. F. Lin, Q. Luo, J. B. Zhao, B. Wang, J. B. Li, Q. Shao, X. K. Guo, N. Wang and Z. H. Guo, *ChemElectroChem*, 2017, DOI: 10.1002/celc.201700816, in press.
12 T. Tatsuma, S. Tachibana, T. Miwa, D. Tryk and A. Fujishima, *J. Phys. Chem. B*, 1999, **103**(38), 8033–8035.
13 A. Mills and J. S. Wang, *J. Photochem. Photobiol., A*, 1999, **127**(1–3), 123–134.
14 S. Yamazaki and N. Nakamura, *J. Photochem. Photobiol., A*, 2008, **193**(1), 65–71.
15 S. Sohrabnezhad, *Spectrochim. Acta, Part A*, 2011, **81**(1), 228–235.
16 W. S. Wang, M. M. Ye, L. He and Y. D. Yin, *Nano Lett.*, 2014, **14**(3), 1681–1686.
17 S. K. Lee, A. Mills and A. Lepre, *Chem. Commun.*, 2004, **7**, 1912–1913.
18 S. K. Lee, M. Sheridan and A. Mills, *Chem. Mater.*, 2005, **17**(10), 2744–2751.
19 A. Mills, A. Belghazi, R. H. Davies, D. Worsley and S. J. Morris, *J. Photochem. Photobiol., A*, 1994, **79**(1–2), 131–139.
20 W. S. Wang, Y. F. Ye, J. Feng, M. F. Chi, J. H. Guo and Y. D. Yin, *Angew. Chem., Int. Ed.*, 2015, **54**(4), 1321–1326.
21 M. Imran, A. Yousaf, X. Zhou, K. Liang, Y. F. Jiang and A. W. Xu, *Langmuir*, 2016, **32**(35), 8980–8987.
22 W. G. Tu, Y. C. Li, L. B. Kuai, Y. Zhou, Q. F. Xu, H. J. Li, X. Y. Wang, M. Xiao and Z. G. Zou, *Nanoscale*, 2017, **9**(26), 9065–9070.
23 J. Hu, Z. K. Guo, P. Mcwilliams, J. Darges, D. Druffel, A. Moran and S. Warren, *Nano Lett.*, 2016, **16**(1), 74–79.
24 H. D. Li, Y. N. Wang, G. H. Chen, Y. H. Sang, H. D. Jiang, J. T. He, X. Li and H. Liu, *Nanoscale*, 2016, **8**(11), 6101–6109.
25 A. Rai, A. Valsaraj, A. Roy, R. Ghosh, S. Sonde, S. Kang, J. Chang, T. Trivedi, R. Dey, S. Guchhait, S. Larentis, L. Register, E. Tutuc and S. Baneryee, *Nano Lett.*, 2015, **15**(7), 4329–4336.
26 C. X. Wang, H. H. Lin, Z. Y. Liu, J. P. Wu, Z. Z. Xu and C. Zhang, *Part. Part. Syst. Charact.*, 2016, **33**(4), 221–227.
27 M. M. Ali and K. N. Y. Sandhya, *New J. Chem.*, 2016, **40**(9), 8123–8130.
28 L. Cao, R. Wang, D. X. Wang, X. Y. Li and H. Y. Jia, *Mater. Lett.*, 2015, **160**, 286–290.
29 H. Feng, N. Tang, S. B. Zhang, B. Liu and Q. Y. Cai, *J. Colloid Interface Sci.*, 2017, **486**, 58–66.
30 M. X. Sun, Y. Wang, Y. L. Fang, S. F. Sun and Z. S. Yu, *J. Alloys Compd.*, 2016, **684**, 335–341.
31 N. Shao, J. N. Wang, D. D. Wang and P. Corvini, *Appl. Catal., B*, 2017, **203**, 964–978.
32 X. F. Liu, Z. P. Xing, Y. Zhang, Z. Z. Li, X. Y. Wu, S. Y. Tan, X. J. Yu, Q. Zhu and W. Zhou, *Appl. Catal., B*, 2017, **201**, 119–127.
33 W. Y. Gao, M. Q. Wang, C. X. Ran and L. Li, *Chem. Commun.*, 2015, **51**(9), 1709–1712.
34 B. Pourabbas and B. Jamshidi, *Chem. Eng. J.*, 2008, **138**(1–3), 55–62.
35 H. Y. He, J. H. Lin, W. Fu, X. L. Wang, H. Wang, Q. S. Zeng, Q. Gu, Y. M. Li, C. Yan, B. K. Tay, C. Xue, X. Hu, S. Pantelides, W. Zhou and Z. Liu, *Adv. Energy Mater.*, 2016, **6**(14), 252–258.
36 R. Lin, Z. H. Zhu, X. Yu, Y. Zhong, Z. L. Wang, S. Z. Tan, C. X. Zhao and W. J. Mai, *J. Mater. Chem. A*, 2017, **5**(2), 814–821.

37 Y. J. Yuan, Z. J. Ye, H. W. Lu, B. Hu, Y. H. Li, D. Q. Chen, J. S. Zhong, Z. T. Yu and Z. G. Zou, *ACS Catal.*, 2016, **6**(2), 532–541.
38 S. Bai, L. M. Wang, X. Y. Chen, J. T. Du and Y. J. Xiong, *Nano Res.*, 2015, **8**(1), 175–183.
39 W. S. Wang, N. Xie, L. Heand and Y. D. Yin, *Nat. Commun.*, 2014, **5**, 5459.
40 W. S. Wang, J. Feng, Y. F. Ye, F. L. Lyu, Y. S. Liu, J. H. Guo and Y. D. Yin, *Nano Lett.*, 2017, **17**(2), 755–761.
41 K. Doushita and T. Kawahara, *J. Sol-Gel Sci. Technol.*, 2001, **22**(1–2), 91–98.
42 T. Z. Lin, B. T. Kang, M. Jeon, C. Huffman, J. Jeon, S. Lee, W. Han, J. Y. Lee, S. Lee, G. Yeom and K. Kim, *ACS Appl. Mater. Interfaces*, 2015, **7**(29), 11589–15892.